OXFORD

ORIGINAL ARTICLE

Altered secondary structure of Dynorphin A associates with loss of opioid signalling and NMDA-mediated excitotoxicity in SCA23

Cleo J.L.M. Smeets[1] Justyna Zmorzyńska[1], Manuel N. Melo[2], Anita Stargardt[3], Colette Dooley[4], Georgy Bakalkin[5], Jay McLaughlin[6], Richard J. Sinke[1], Siewert-Jan Marrink[2], Eric Reits[3] and Dineke S. Verbeek[1],*

[1]Department of Genetics, University of Groningen, University Medical Centre Groningen, Groningen, the Netherlands [2]Groningen Biomolecular Sciences and Biotechnology Institute, Centre for Life Sciences, University of Groningen, Groningen, The Netherlands [3]Department of Cell Biology and Histology, Academic Medical Centre, Amsterdam, The Netherlands [4]Torrey Pines Institute for Molecular Studies, Port St Lucie, FL, USA [5]Division of Biological Research on Drug Dependence, Department of Pharmaceutical Biosciences, Uppsala University, Uppsala, Sweden and [6]Department of Pharmacodynamics, University of Florida, Gainesville, FL, USA

*To whom correspondence should be addressed at: Email: d.s.verbeek@umcg.nl

Abstract

Spinocerebellar ataxia type 23 (SCA23) is caused by missense mutations in prodynorphin, encoding the precursor protein for the opioid neuropeptides α-neoendorphin, Dynorphin (Dyn) A and Dyn B, leading to neurotoxic elevated mutant Dyn A levels. Dyn A acts on opioid receptors to reduce pain in the spinal cord, but its cerebellar function remains largely unknown. Increased concentration of or prolonged exposure to Dyn A is neurotoxic and these deleterious effects are very likely caused by an *N*-methyl-D-aspartate-mediated non-opioid mechanism as Dyn A peptides were shown to bind NMDA receptors and potentiate their glutamate-evoked currents. In the present study, we investigated the cellular mechanisms underlying SCA23-mutant Dyn A neurotoxicity. We show that SCA23 mutations in the Dyn A-coding region disrupted peptide secondary structure leading to a loss of the N-terminal α-helix associated with decreased κ-opioid receptor affinity. Additionally, the altered secondary structure led to increased peptide stability of R6W and R9C Dyn A, as these peptides showed marked degradation resistance, which coincided with decreased peptide solubility. Notably, L5S Dyn A displayed increased degradation and no aggregation. R6W and wt Dyn A peptides were most toxic to primary cerebellar neurons. For R6W Dyn A, this is likely because of a switch from opioid to NMDA- receptor signalling, while for wt Dyn A, this switch was not observed. We propose that the pathology of SCA23 results from converging mechanisms of loss of opioid-mediated neuroprotection and NMDA-mediated excitotoxicity.

Introduction

Missense mutations in prodynorphin (*PDYN*) cause spinocerebellar ataxia type 23 (SCA23), an autosomal dominant disorder in which patients suffer from relatively slowly progressive motor co-ordination impairment because of atrophy of the cerebellum characterized by pronounced Purkinje cells loss (1,2). PDYN

is the precursor protein for the opioid neuropeptides α-neoendorphin, Dynorphin (Dyn) A and Dyn B, which are inhibitory neurotransmitters and function in pain processing, stress-induced responses and addiction control (3–6). Dyn A acts on opioid receptors and preferentially binds to the κ-opioid receptor (KOR) but can also interact with the μ-opioid receptor (3). While the role of Dyn A has been extensively studied in pain, stress and addiction, the cerebellar function of this peptide, by which SCA23-mutant Dyn A can mediate an ataxic phenotype, is largely unknown.

Evidence is accumulating that pathophysiological changes in Dyn A production, concentration or processing can contribute to maladaptive neuroplastic changes and neurodegeneration [reviewed in (4)]. The deleterious effect of Dyn A seen in secondary neuronal injury is mediated through non-opioid mechanisms as it cannot be blocked by opioid antagonists (7). The finding that MK801, a specific blocker of the *N*-methyl-D-aspartate (NMDA) receptor, is able to prevent the negative consequences of elevated concentrations of or prolonged exposure to Dyn A, indicates that non-opioid mechanisms of Dyn A are mediated via this receptor (8). Dyn A peptides were shown to bind NMDA receptors and potentiate their glutamate currents (9). The dichotomous effects of Dyn A peptides were proposed by Hauser *et al.* (8) to include neuroprotection through opioid signalling and neurotoxicity via NMDA receptor activation. The neuroprotection mediated via Dyn A interaction with KOR relies on reduction of intracellular calcium concentrations upon KOR activation by Dyn A (10,11), while the neurodegenerative actions mediated by NMDA receptor activation involve excitotoxic mechanisms and pathological calcium increase in neurons upon stimulation.

Structure–activity analyses of Dyn A, consisting of 17 amino acids, indicate that Tyr[1], Leu[5] and Arg[6]–Lys[11] are required for KOR binding efficiency (12,13). Interestingly, the SCA23 mutations that are localized to the Dyn A-coding region (L5S, R6W and R9C) alter these amino acids (2). Receptor binding requires a properly structured Dyn A peptide containing a stable N-terminal α-helical structure, from Phe[4] to Pro[10], and a relatively unstable C-terminal β-turn, formed by amino acids Trp[14] to Gln[17] (14). However, Dyn A is likely unfolded in an aqueous environment, and only folds when in a membrane environment (15). Therefore, we suggest that membrane interaction of Dyn A precedes and facilitates receptor binding.

Previously, we showed that mutant PDYN-L211S and -R212W expressed in a cell model, and PDYN-R212W in mice, lead to enhanced levels of mutant Dyn A peptide (2,16). This work points to a crucial role for mutant Dyn A in the underlying mechanism of SCA23. Additionally, the R6W and R9C Dyn A peptides induced toxicity above that of wild-type Dyn A in cultured mouse striatal neurons, in contrast to the L5S mutant, which did not exhibit increased neurotoxic activity (2). Here, we have studied the impact of the SCA23 mutations on Dyn A to reveal the molecular mechanisms underlying SCA23-mutant Dyn A toxicity.

Materials and Methods

Modelling of secondary structure and interaction of Dyn A with POPC membranes

The interaction of Dyn A mutants with palmitoyl-oleyl phosphatidylcholine (POPC) membranes was simulated using the GROMACS software package version 4.5 or 5.1, the GROMOS43A1 force field, and parameters for the phospholipids adapted from Pronk *et al.* (17) and Berger *et al.* (18). Simulations were carried out at 310 K and 1 bar for at least 200 ns, at a time step of 1 fs. The Berendsen thermostat and barostat (19) were used at 0.1 and 0.5 ps coupling times, respectively. The systems were composed by a single peptide molecule, a 104 POPC membrane patch, 3428 water molecules and either 3 or 4 countering chloride ions depending on the formal charge of the mutant. Prior to production runs, the system with the Dyn A–wt peptide was equilibrated for 5 μs using the MARTINI coarse-grain force field (20). In the coarse-grain simulations, the secondary structure of wt Dyn A was restrained to reproduce the structural propensities reported by Tessmer and Kallic (21). The mutations/deletion were also performed at the (more robust) coarse-grain level, after which the system was again briefly equilibrated for 2 ns before being converted to a fine-grained representation following the procedure described in Rzepiela *et al.* (22). At the fine-grain level, the systems were energy-minimized and then equilibrated for 0.5 ns at constant volume and a 0.5 fs time step, with a temperature coupling time of 0.01 ps. A second equilibration step was performed for 1 ns at a 1 fs time step with 0.1 ps temperature coupling time and 0.05 ps pressure coupling time. Four replicate simulations were performed for each peptide, obtained by reassigning particle velocities to values randomly extracted from a Maxwell–Boltzmann distribution at 310 K; replication and velocity reassignment was done prior to the second equilibration step. Secondary structure analysis was done using the DSSP tool [CMBI version of April 4, 2000 (23)]. Visualization was done using the VMD package (24).

Peptide synthesis

SCA23-mutant and wt Dyn A peptides were synthesized by solid phase strategies using an automated multiple peptide synthesizer (SyroII, MultiSyntech). For the quenched Dyn A peptides, a cysteine was inserted into the Dyn A sequence in between two glycines at the N-terminus and a fluorescein (Fl) was introduced by covalent coupling of fluorescein-5-iodoacetamide (5-IAF, Fluka) to the cysteine. Quenching of Fl fluorescence was performed by a dabcyl group that had been introduced in the peptide by coupling of Fmoc-L-Lys (Dabcyl)-OH (NeoMPS). Peptides were purified by the size exclusion chromatography and the reversed phase-HPLC (>95% pure) and showed the expected molecular mass as determined by the mass spectrometry (Maldi Tof, Voyager, ABI). Peptides were dissolved in 100% 1,1,1,3,3,3-hexafluoro-2-propanol (HFIP; Sigma), aliquoted, dried under vacuum in a SpeedVac (Eppendorf) and stored at −20 °C.

KOR competitive binding assay

The competitive binding assay of Dyn A peptides to KOR was performed as described previously (25). Briefly, the Dyn A competitive binding was assessed in the presence of radioactively labelled U69 593 as a competitor in rat cerebellar membrane fraction. Different concentrations of Dyn A peptide were tested. Unlabelled U50 488 was used to decrease unspecific binding and generate standards. Bound radioactivity was counted on a Wallac Beta-plate Liquid Scintillation Counter (Piscataway). Non-linear regression analysis of the competition curves was fit by using Graphpad Prism Software, assays were conducted by using two replicates and were repeated for four times. The averaged K_i values for the four experiments were subjected to One way ANOVA followed by Dunnett's multiple comparison using DynA wt as standard.

Quenched Dyn A peptide degradation assay

The degradation assay was performed as described previously (26). Briefly, HFIP-treated aliquots of Dyn A peptides were resuspended in DMSO followed by sonication for 10 min, immediately before addition to 5 μg protein from the mouse cerebellum extracts or cerebrospinal fluid (CSF) in KMH buffer (110 mM KAc, 2 mM MgAc and 20 mM Hepes–KOH, pH 7.2) to a total volume of 50 μl. Degradation of the peptide was analysed at 37 °C using a fluorescence plate reader (FLUOstar OPTIMA, BMG Labtec.).

Electron microscopy

Dyn A peptide (150 ng/ml in water) preparations were adsorbed on 300-mesh formar/copper grids for 2 min and the excess of fluid was filtered off. Upon staining with 2.5% uranyl acetate for 2 min, grids were analysed with a transmission electron microscope (Tecnai-12 G2, FEI). Aggregates were quantified using ImageJ software.

Primary cell culturing

Cerebella were dissected from 4- to 6-day-old C57/Bl6 mouse pups, and kept in ice cold sterile PBS (Gibco, Life Technologies), supplemented with 0.3% bovine serum albumin (Sigma) and 0.6% glucose. After dissection, the meninges were removed without rupturing the tissue. Cerebella were then incubated in warm trypsin for 10 min and mechanically dissociated in DMEM medium (Gibco, Life Technologies), supplemented with 10% fetal bovine serum (Gibco, Life Technologies), 0.25% penicillin/streptomycin (Gibco, Life Technologies), 0.25% glutamine (Gibco, Life Technologies) and DNAse I (Sigma). After at least two dissociation cycles, the neurons were plated in dissociation medium without DNAse I for 1 h to remove glia from the cell suspension. Neurons were then plated into 24-well plates coated with poly-D-lysine, with 200 000 cells per well in Neurobasal culture medium (Gibco, Life Technologies), supplemented with B-27 (Gibco, Life Technologies), 0.25% penicillin/streptomycin, 0.25% glutamine and 0.5% fetal bovine serum. After 24–48 h of culturing, 0.5 μM Ara-C (Sigma) was added to the cultures to inhibit the growth of any remaining glial cells. Cultures were then allowed to mature in medium (with Ara-C) for 10–14 days as described in (27).

Peptide-induced lactate dehydrogenase activity assay

Mature cerebellar cultures expressing *Kor*, *Mor*, *Pdyn*, various excitatory amino acid receptors, *GluN1*, *GluN2b* and *GluR1* (data not shown; 27,28) were stimulated with 100 nM Dyn A (wt, L5S, R6W or R9C) dissolved in sterile saline, and 25 μl of the medium was collected at each time point, spun down for 10 min at 13 000 rpm (radius 9.5 cm) and 4 °C, and stored at −80 °C for analysis. The time points were t0 (before addition of peptide), t1 (1 h after addition of peptide), t3, t6, t12, t24, t48 and t72. Negative controls consisted of no stimulation and stimulation with saline, and cell dysfunction and death was induced by stimulation with 10 μM EDTA (Gibco, Life Technologies) as a positive control. After the collection of all samples, the lactate dehydrogenase (LDH) activity was measured with an LDH Activity Kit (Sigma) and was performed according to the manufacturer's protocol. Blocking of peptide-induced toxicity was achieved via 30 min of pretreatment with 10 μM of either naloxone (opioid receptor block, Sigma) or MK-801 (NMDA receptor block, Sigma).
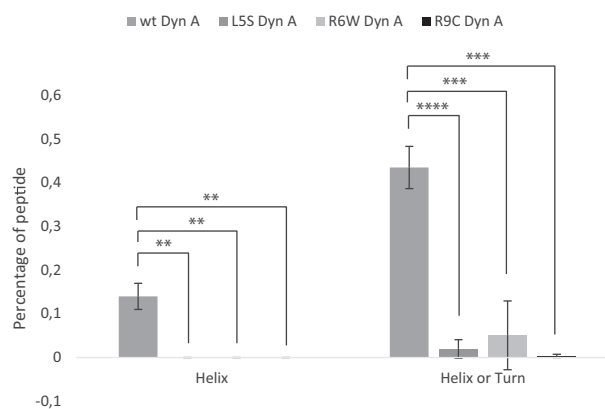

Figure 1. SCA23-mutant Dyn A peptides lose crucial α-helix secondary structure. Histogram of the percentage of helical (α- + 3-helix) and helical + turn structure within each peptide over the simulation time (turns being a simpler element of higher order secondary structure). While wt Dyn A residues were in an α-helical conformation ∼14% of the time, and in a helical or turn configuration ∼43% of the time, the SCA23-mutant Dyn A peptides did not show any α-helical structure at all, and only small amounts of turn. Significant differences are indicated as **$p < 0.,01$, ***$p < 0.001$ and ****$p < 0.0001$.

Statistical analysis

All data are expressed as mean ± SEM of at least three independent experiments. Statistical significance was tested using unpaired Student's *t*-test, unless stated otherwise.

Results

SCA23 mutations disrupt the secondary structure of Dyn A peptides

To gain insight into the mechanisms underlying SCA23 mutations in the Dyn A-coding region, we first examined the impact of these mutations—including L5S, R6W and R9C—on the secondary structure of Dyn A peptides by computational modelling of the peptides in the presence of membrane. The simulation was carried out for at least 200 ns, enabling us to follow the stability of peptide secondary structures in time. In POPC membranes, the wt Dyn A peptide kept a stable N-terminal α-helix configuration from residues Phe[4] to Arg[9] (Fig. 1 and Supplementary Material, Fig. S1A). This is in agreement with several previous structural characterizations of the peptides (21,29,30) and validates our modelling approach. The wt Dyn A secondary structure was stable across the entire simulation time. The SCA23 mutations in Dyn A peptides resulted in a loss of the N-terminal α-helical structure (Fig. 1 and Supplementary Material, Fig. S1B–D), even during the equilibration procedure, suggesting that amino acids Lys[5], Arg[6] and Arg[9] are essential for the stabilization of the α-helix. The in-depth membrane profile of each peptide upon interaction with POPC was also monitored. R6W Dyn A underwent the largest change in in-depth positioning relative to wt Dyn A, with a deeper positioning of Arg[6] and a shallower positioning between Ile[8]–Gln[17] in the membrane (Fig. 2A). In-depth positioning of L5S Dyn A relative to wt Dyn A only changed significantly at Ser[5], while R9C Dyn A did not show any significant change (Fig. 2A). Additionally, flexibility of the peptides was measured as the root-mean-square-fluctuation of the backbone atom positions. All mutants displayed overall greater structural flexibility than wt Dyn A, with peptides L5S and R6W Dyn A displaying the most significant differences (Fig. 2B). This is in line with the poorly defined structure of the mutants.
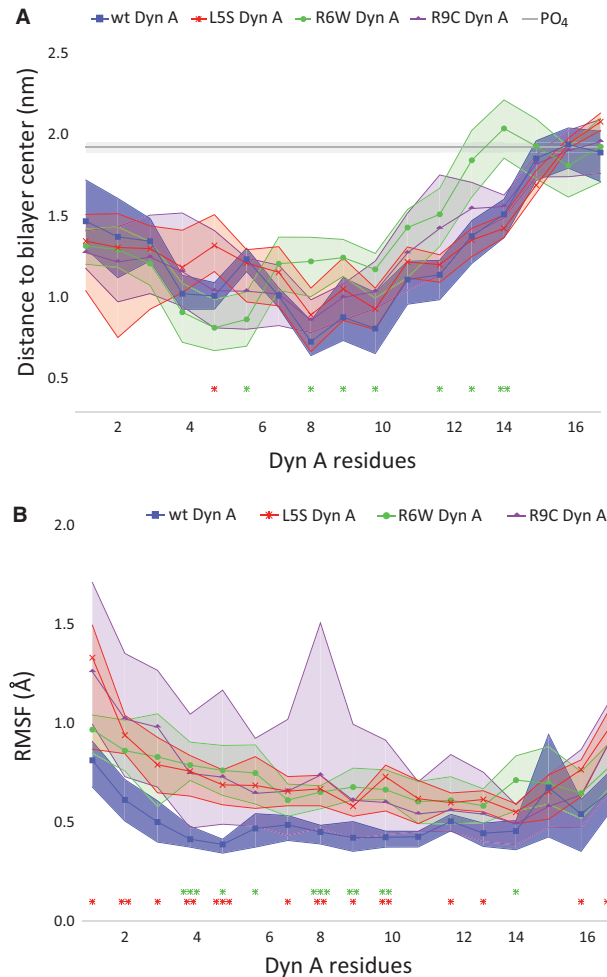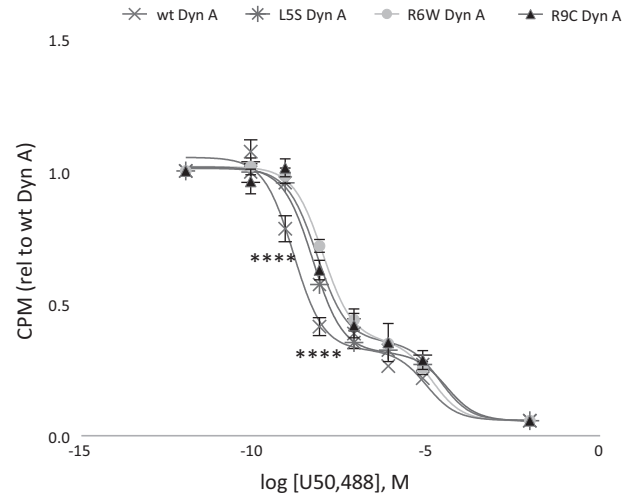
Figure 3. SCA23-mutant Dyn A peptides display reduced affinity to KOR. Quantification graph of competitive binding assays between the various Dyn A peptides and the highly selective KOR ligand U69, 593. All SCA23-mutant Dyn A peptides exhibited lower potential to displace the antagonist from the high affinity binding site when compared with wt Dyn A. Data are shown as a mean of four independent experiments ($\pm$SEM). Significant differences are indicated as ****$p < 0.0001$.

Figure 2. Altered SCA23-mutant Dyn A peptide membrane positioning and flexibility. Membrane positioning and flexibility of the various modelled Dyn A peptides. (**A**) Membrane positioning is displayed as the average distance of Cα carbons of each residue of wt and SCA23-mutant Dyn A peptides to the centre of the POPC bilayer. The insertion depth of L5S and R9C Dyn A peptides seems to be little affected during the studied time scale. R6W Dyn A is positioned significantly more shallow in the membrane, specifically between Arg[7] and Asp[15]. (**B**) Peptide flexibility is displayed as the root-mean-square-fluctuation of peptide backbone atom positions during the time scale studied. All mutants show a greater structural flexibility than wt, to varying degrees of significance. The analysis was carried out for the last 80 ns of each replicate simulation. In (A), the grey line indicates the average position of phosphate groups. Shaded regions around each line indicate 95% confidence intervals; asterisks below each data point indicate significant difference to the wt Dyn A value. Significant differences are indicated as *$p < 0.05$, **$p < 0.01$ and ***$p < 0.005$.

Altogether, these data show that SCA23 mutations disrupt the native conformation of Dyn A, R6W Dyn A positions higher in the membrane, and all mutants display increased flexibility. These factors can be expected to affect in-membrane binding to the KOR, either through a lower affinity of the receptor because of a destructured N-terminal signal sequence and increased peptide flexibility, or by in-depth misalignment of the two.

SCA23-mutant Dyn A peptides exhibit reduced KOR affinities

As the SCA23 mutations affect amino-acids Lys[5], Arg[6] and Arg[9], which are important for KOR binding (12,13), we hypothesized

that SCA23-mutant Dyn A peptides may exhibit decreased receptor affinity. To test this hypothesis, we analysed the KOR binding of the various mutant Dyn A peptides *in vitro* in a competitive binding assay using selective KOR ligand (^{3}H-U69 593) as a competitor. The competition analysis showed that SCA23-mutant Dyn A peptides have significantly lower KOR affinity than wt Dyn A. Values $K_i \pm$ SEM: L5S: 2.9 ± 0.9 nM, R6W: 7.9 ± 2.1 nM and R9C: 3.8 ± 0.7 nM versus wt: 0.69 ± 0.13 nM, respectively (Fig. 3), as hypothesized. These data indicate that the partial loss of KOR signalling might contribute to the SCA23 pathology.

The disruption of the α-helix in Dyn A is a likely factor for the loss of KOR affinity by the SCA23-mutant Dyn A peptides. To further test this hypothesis we also simulated in a membrane the Y1del Dyn A mutant, lacking Tyr[1], that is known to have no affinity to opioid receptors, including KOR, and exhibits only non-opioid functions (31). Our results showed that, as observed for the various SCA23-mutant Dyn A peptides, Y1del Dyn A is also missing the N-terminal α-helical structure (Supplementary Material, Fig. S2A and B). Additionally, a shift in Y1del Dyn A positioning in the membrane was seen between Ile[8] and Trp[14] (Supplementary Material, Fig. S2C), similar to the shift seen in R6W Dyn A positioning (Fig. 2). However, while both Y1del and SCA23-mutant Dyn A peptides displayed disruption of the N-terminal α-helix, the latter still bound KOR much more efficiently than the former (28), indicating that the α-helical structure in Dyn A is important for the KOR interaction, but is not its sole determinant. Indeed, an overall greater structural stability of the Y1del Dyn A peptide was observed, closer to the behaviour of the wt Dyn A peptide (Supplementary Material, Fig. S2D), and this might be a factor towards KOR interaction.

SCA23 mutations affect the degradation efficiency and aggregation of Dyn A peptides

As SCA23 mutations disrupt the native conformation of Dyn A, we hypothesized that alterations in the secondary structure of SCA23-mutant Dyn A affect proper peptide degradation. To test
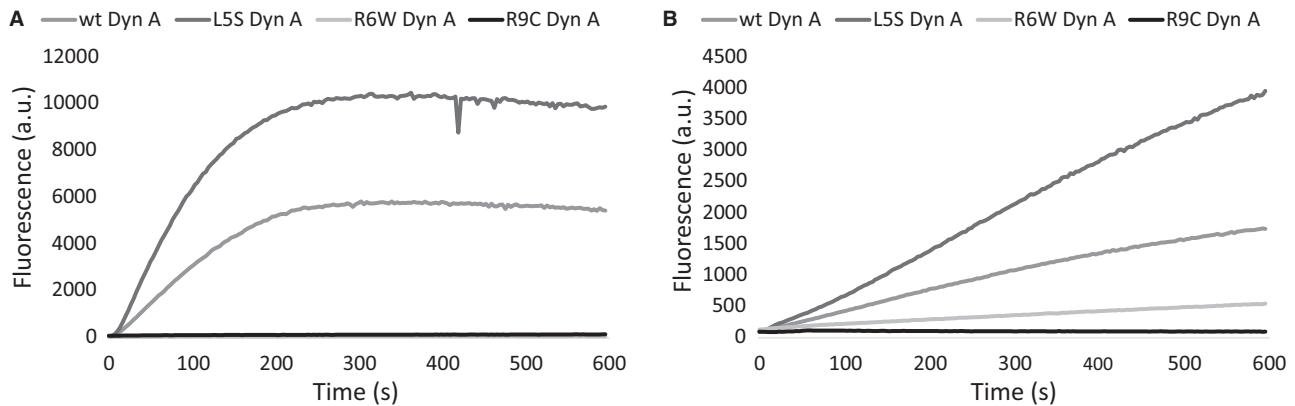
Figure 4. Altered degradation rates of SCA23-mutant Dyn A peptides. Degradation curves of wild-type and SCA23-mutant Dyn A peptides in time as measured by increases in fluorescence intensity upon separation of the quencher and fluorophore. The assay was carried out in mouse cerebellar extract (**A**) or in CSF (**B**) for 200 cycles of 5 min. L5S Dyn A displays increased degradation in both mouse cerebellar extract and CSF, while both R6W and R9C Dyn A show reduced degradation.
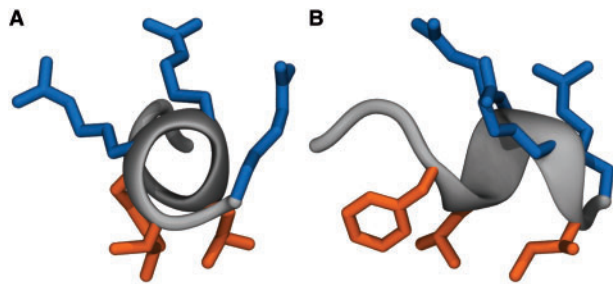

Figure 5. Cationic and hydrophobic residues are separated in wt Dyn A by the α-helix. Front (**A**) and side view (**B**) of residues three to nine of wt Dyn A with explicit side chains around a cartoon representation of the backbone secondary structure. The helical structure separates the cationic Arg[6,7,9] residues (blue) from the hydrophobic Phe[4], Leu[5] and Ile[8] residues (orange). Images were taken aligned with the plane of the membrane.

this, we determined the breakdown of the mutant Dyn A peptides in mouse cerebellar extracts and CSF in real time. For this purpose, we generated Dyn A peptides with a small fluorescent group at the N-terminus and a quenching dabcyl group introduced to medial/C-terminal part of Dyn A peptides (32). The quenched Dyn A peptides become fluorescent upon separation of the fluorophore and quencher owing to degradation of the peptide. In mouse cerebellar extracts, rapidly increasing fluorescence levels were observed for wt Dyn A and L5S Dyn A, but not for R6W Dyn A and R9C Dyn A (Fig. 4A), reflecting markedly reduced degradation of these mutant peptides. Notably, L5S Dyn A was more rapidly degraded than wt Dyn A. We also determined peptide stability in CSF, which contains many metabolic enzymes, including hydrolases and peptidases. Under these conditions, the degradation of wt Dyn A and L5S Dyn A was less rapid than in cerebellar extract, but similar profiles were generated for all peptides, validating our previous findings (Fig. 4B). These data clearly showed that the R6W and R9C mutations impair Dyn A degradation, whereas the L5S mutation seems to increase Dyn A breakdown. Impaired peptide degradation, combined with increased precursor processing (16), is a likely cause of increased peptide levels (2,16). Furthermore, the more efficient degradation of wt Dyn A and L5S Dyn A peptides in cerebellar extract compared with CSF, suggests the presence of neuronal-tissue-specific peptidases in cerebellum that degrade this peptide with higher efficiency.

As the SCA23 mutations markedly disrupt the wt Dyn A secondary structure, desegregating hydrophobic and cationic residues (Fig. 5A and B), it is admissible that the resulting 'denatured' structures have lower solubility. Therefore, we investigated the *in vitro* oligomerization of SCA23-mutant Dyn A peptides in time by the electron microscopy. Initially, all three SCA23-mutant peptides displayed more oligomeric structures than wt Dyn A (Fig. 6A–D and U). While wt, R6W and R9C Dyn A continued to form oligomeric structures over time, L5S Dyn A oligomerization did not change (Fig. 6E–U). An increased number of oligomeric structures was observed for R6W and R9C Dyn A after 4 h of incubation when compared with wt and L5S Dyn A, indicating a higher oligomeric potential for R6W and R9C Dyn A.

Altogether, these data indicate that R6W and R9C Dyn A have an increased half-life because of decreased degradation. These stable R6W and R9C Dyn A peptides display a lower solubility than wt and L5S Dyn A, likely affecting the membrane solubility and self-interaction. L5S Dyn A is characterized by rapid degradation and little aggregation, which may underlie its lower neurotoxicity compared with R6W and R9C Dyn A, observed in striatal neurons (2).

SCA23-mutant Dyn A display increased neurotoxic effects via NMDA receptor

Recent work has shown that Dyn A non-covalently binds NMDA receptors and can potentiate their excitatory currents (9). Additionally, high concentrations of or prolonged exposure to Dyn A has been shown to cause neuronal cell death via non-opioid mechanisms (7,8). Given the elevated mutant Dyn A levels in SCA23 pathology (2,16), and cell death caused *in vitro* (2), we hypothesized that the mutant peptides may induce neuronal dysfunction through NMDA receptor activation, and subsequent cell death. To reveal the neurotoxicity of the SCA23-mutant peptides, mature primary mouse cerebellar cultures of 10–14 days *in vitro* (DIV) were treated with exogenously added peptides (100 nM), and lactase dehydrogenase (LDH) activity was measured in time up to 72 h post-treatment. Notably, R9C Dyn A was already significantly more toxic to primary neurons at 100 nM after 3 h of treatment than all other peptides (Fig. 7A and B). However, after 6, and up to 72 h, all peptides were toxic as shown by significantly increased LDH activity, and wt and R6W Dyn A increased LDH activity most at 72 h (Fig. 7A and B).
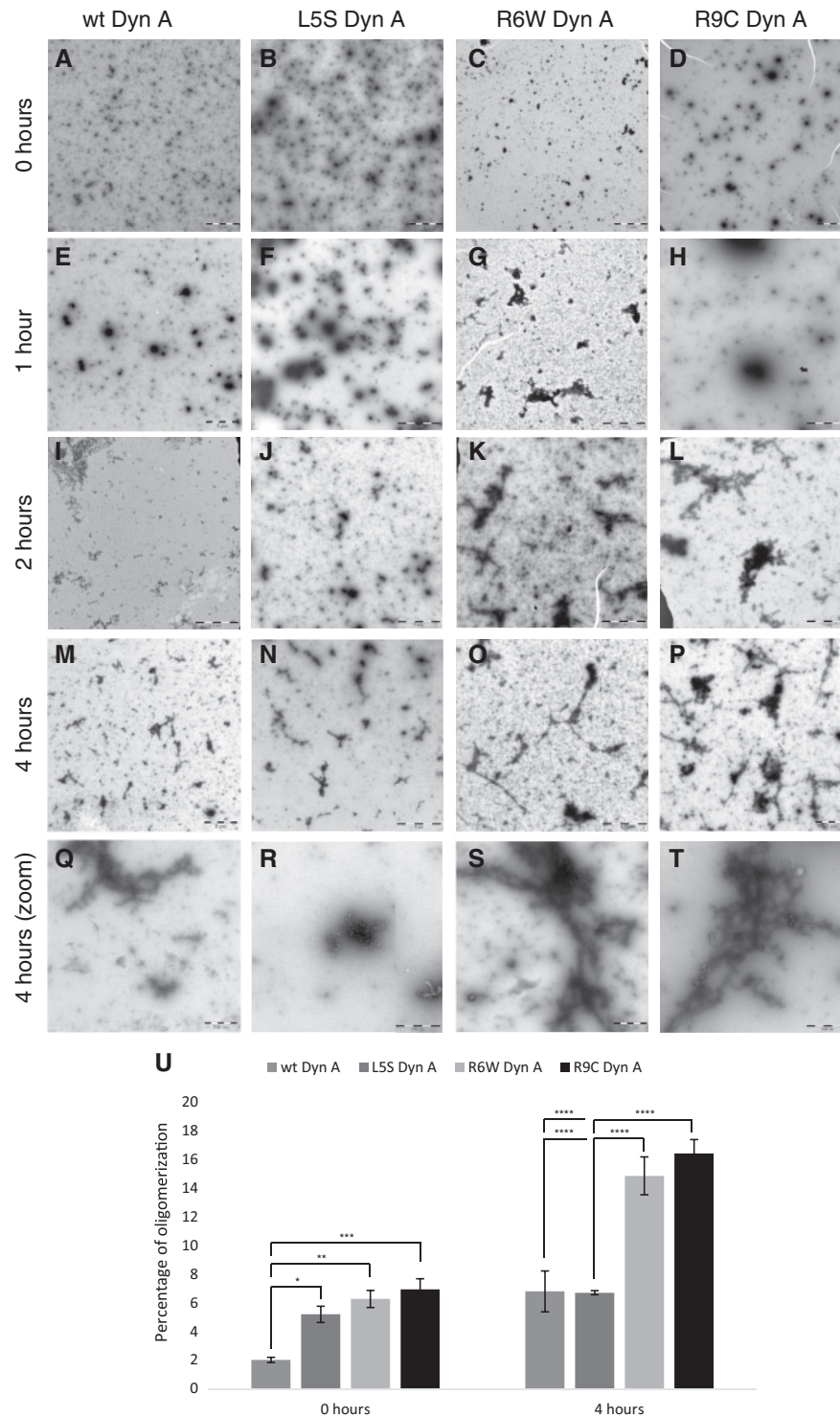
Figure 6. Changes in oligomerization of SCA23-mutant Dyn A peptides in time. Electron microscopy images showing oligomerization of Dyn A peptides at 37 °C in time (0–4 h). Scale bars of (**A**)–(**D**) in μm, (**E**)–(**P**) 5 μm, (**Q**)–(**T**) 500 nm. (**U**) Quantification of Dyn A oligomerization demonstrated that while at 0 h, all three mutant Dyn A peptides displayed more aggregation, at 4 h, R6W and R9C Dyn A oligomerized more than wt or L5S Dyn A. Over time, wt, R6W and R9C Dyn A demonstrated significantly increased aggregation (wt Dyn A $p < 0.01$, R6W Dyn A $p < 0.0001$, R9C Dyn A $p < 0.0001$), while L5S Dyn A aggregation did not change. Significant differences (two-way ANOVA) are indicated as $^*p < 0.05$, $^{**}p < 0.01$, $^{***}p < 0.001$ and $^{****}p < 0.0001$.

Additionally, all peptides caused cell death at 72 h upon Dyn A peptide treatment compared with saline treated cerebellar neurons (Supplementary Material, Fig. S3).

To determine which receptor system mediates the neuronal dysfunction caused by Dyn A, we pre-treated primary cerebellar neurons with 10 μM of either naloxone or MK801 for 30 min in order to block opioid-mediated or NMDA-mediated toxicity, respectively. Pre-treatment of both naloxone and MK801 seemed to lower overall toxicity, as Dyn A induced LDH levels of pre-treated cells were lower than those without pre-treatment. Wt
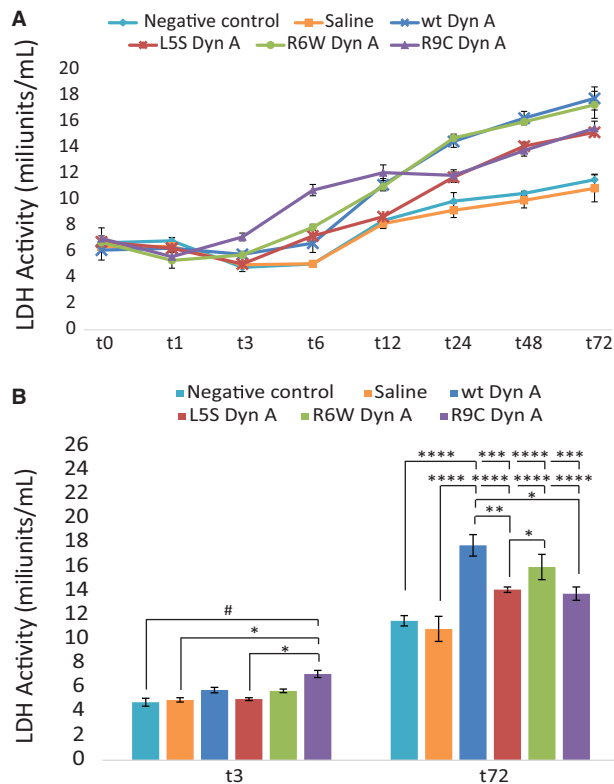
Figure 7. Wt and SCA23-mutant Dyn A peptides cause dysfunction of primary cerebellar neurons at 100 nM. Quantification of LDH activity of primary cerebellar cultures in the presence of various Dyn A peptides in time, showing high toxicity for all Dyn A peptides. Wt and R6W Dyn A induced the highest levels of LDH activity. (**A**) 100 nM Dyn A peptide was added to primary cultures, and LDH activity was monitored for 72 h. These data are presented as mean ± SEM. (**B**) Representation of t3 and t72. Significant differences are indicated as #0.10 > p > 0.05, *p < 0.05, **p < 0.01, ***p < 0.001 and ****p < 0.0001.

Dyn A toxicity was not affected differently by either pre-treatment over the full time course, with the exception that naloxone pre-treatment led to higher LDH activity at 24 h, compared with MK801 pre-treatment (Fig. 8A). Both pre-treatments initially delayed R6W Dyn A toxicity, whereas at 72 h, MK801 pre-treatment led to lower R6W Dyn A induced LDH levels than naloxone pre-treatment (Fig. 8B). R9C Dyn A toxicity was not delayed by either pre-treatment, while MK-801 pre-treatment also reduced R9C Dyn A induced LDH levels at 72 h (Fig. 8C). In contrast, MK-801 pre-treatment initially decreased toxicity of L5S Dyn A, naloxone pre-treatment decreased L5S Dyn A induced LDH levels at 12, 48 and 72 h when compared with MK801 pre-treatment (Fig. 8D).

Overall, in our model, all Dyn A peptides cause cellular dysfunction and cell death at 100 nM, with R6W and wt Dyn A being most potent, and L5S Dyn A being least efficient. Additionally, the SCA-mutant Dyn A peptides likely interact with both opioid and NMDA receptors, and our data suggest that R6W Dyn A toxicity is mainly mediated via NMDA receptors, while that of L5S Dyn A is mainly opioid mediated. Furthermore, blocking of the opioid receptors seems to inhibit opioid-induced neuroprotection.

Discussion

In the present study, we showed that both loss of opioid signalling and gained NMDA receptor activation underlies

neuronal cell death in SCA23. The secondary structure of the SCA23-mutant peptides showed marked changes, and R6W Dyn A displayed similarities with the secondary structure of Y1del Dyn A, lacking KOR binding and opioid activity (31). Likewise, the SCA23-mutant peptides showed reduced KOR binding affinity, and peptide toxicity, in part, mediated via the NMDA receptor leading to cellular dysfunction and cell death. Additionally, increased Dyn A peptide stability and subsequent reduced peptide solubility very likely underlies a large part of the elevated mutant Dyn A levels previously observed in our SCA23 disease models (2,16), in addition to increased precursor processing (16). An overview of the changes can be found in Table 1.

The loss of the N-terminal α-helix in the Dyn A secondary structure caused by the SCA23 mutations and deletion of Tyr[1] demonstrates that these amino acids are crucial for α-helix formation. Since the SCA23-mutant Dyn A peptides exhibit reduced KOR affinity, whereas Y1del Dyn A has no remaining opioid activity, we suggest that the N-terminal α-helix plays a crucial role in the positioning of the peptide for interaction with the opioid receptors, but that it is not the sole determinant of proper receptor binding. Moreover, the altered secondary structures may contribute to the formation of stable oligomeric structures *in vitro*, as the R6W and R9C mutations in particular desegregate hydrophobic and cationic residues, lowering their solubility, a characteristic that was absent in L5S Dyn A peptides. However, serine at position 5 of Dyn A may introduce a novel phosphorylation site that may promote enhanced degradation of the peptide via proteasome-independent ubiquitination. Additionally, substrates containing a phorphorylated residues adjacent to a proline showed altered proline-specific peptidase cleavage (33), but since Ser[5] is not flanked by a proline on either side, we can only speculate whether this will also be the case for L5S Dyn A. Yet physiological relevance of these findings is hard to assess, as the oligomerization assays were performed in an aqueous solution, i.e. without the presence of membranes. Notably, no oligomeric structures were observed in the cerebella of PDYN-R212W mice that exhibit elevated R6W Dyn A levels (unpublished data). As these mutant peptides may not oligomerize in physiological conditions, these data suggest that R6W and R9C Dyn A peptides may perform additional pathological interactions, either accumulating in higher molecular weight species or interacting with unknown partners. All these effects on Dyn A induced by the SCA23 mutations may contribute to increased neurotoxic actions.

Surprisingly, we did not observe the increased toxicity for R6W and R9C Dyn A compared with wt Dyn A that has been seen before (2) in our current cellular model containing several different cell types, namely mainly granule cells and some basket cells, Golgi cells and Purkinje cells. Therefore, we cannot exclude that Dyn A toxicity in SCA23 is specific for specific populations of neurons, and different effects could be seen for the different cell types, and combinations thereof. Dyn A toxicity was, at least in part, mediated via the NMDA receptor, as blocking the NMDA receptor with MK801 did not completely prevent the cellular dysfunction caused by the various Dyn A peptides. This data validated the work reported previously by others (7,8), and suggests that at least part of the toxicity is non-NMDA- receptor mediated, and in addition to NMDA signalling, the opioid route contributed to the neuronal cell loss induced by SCA23-mutant Dyn A as well. Furthermore, the actions of mutant Dyn A could act via α-amino-3-hydroxy-5-methyl-4-isoxazolepropionic acid (AMPA) or kainite receptors, or acid-sensing ion channels (ASICs) (34,35), which needs to be explored in future work. Additionally, non-receptor mediated actions could
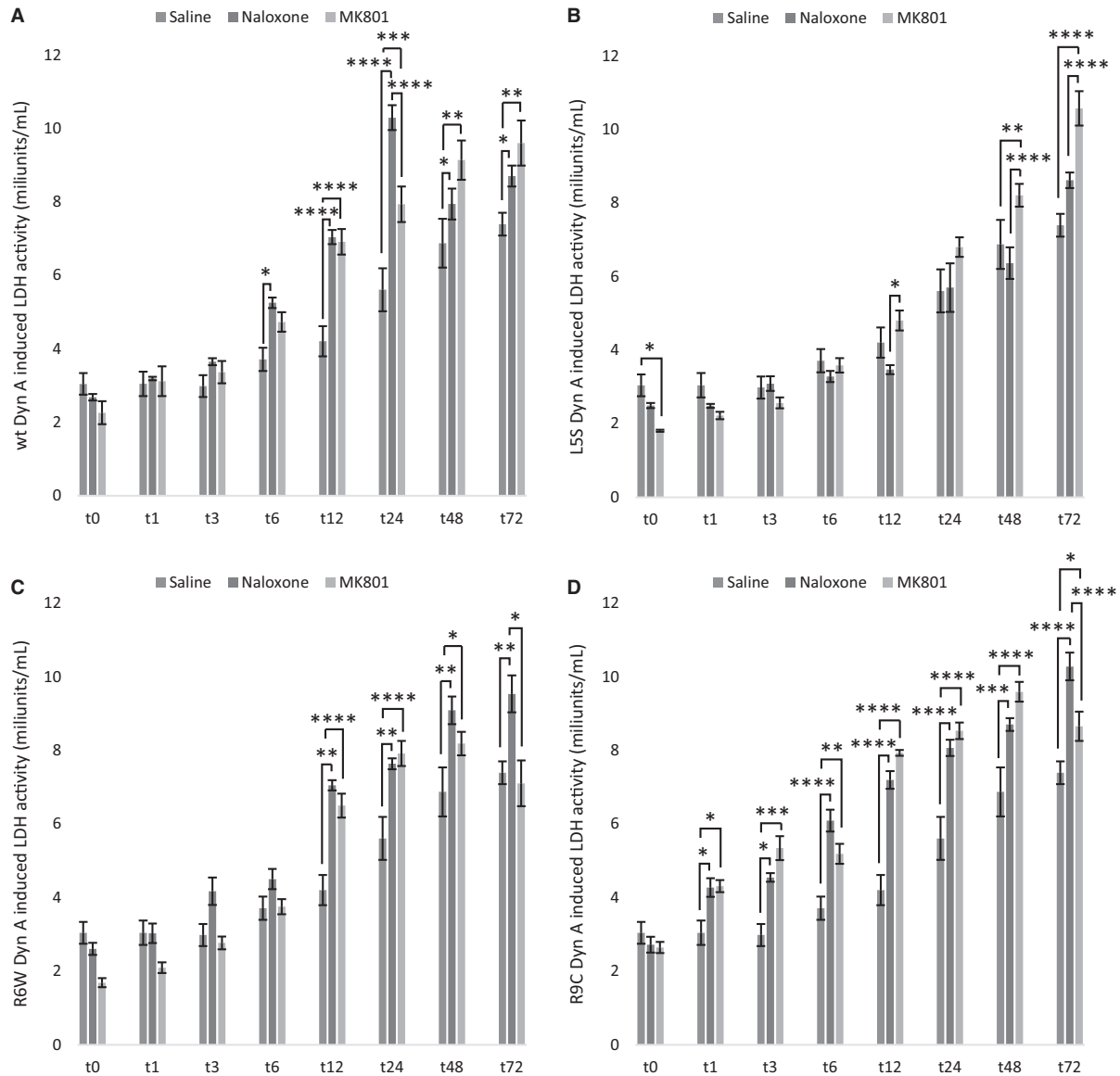
Figure 8. The toxic effects of Dyn A are mediated via both opioid and NMDA receptor interaction. Quantification graphs of LDH activity in the presence of wt (A), L5S (B), R6W (C) and R9C (D) 100 nM Dyn A peptides in time, with 30 min of pre-treatment with either naloxone (10 μM) or MK801 (10 μM). (A) Naloxone pre-treated wt Dyn A only displayed increased toxicity at t24 when compared with MK801 pre-treated wt Dyn A. (B) R6W Dyn A toxicity was significantly reduced by MK801 pre-treatment at t0, t1, t3, t6 and t72. (C) Naloxone pre-treatment reduced R9C Dyn A toxicity at t3, t12, t48, while it increased R9C Dyn A toxicity at t6 and t72. (D) Naloxone pre-treatment increased toxicity of L5S Dyn A at t0, t1 and t3, while it decreased L5S Dyn A toxicity at t12, t48 and t72. These data are presented as mean ± SEM. Significant differences are indicated as $^{\#}$ $0.10 > p > 0.05$, $^{*}p < 0.05$, $^{**}p < 0.01$ and $^{***}p < 0.001$.

underlie Dyn A's neurotoxicity, as wt and mutant Dyn A have been shown to penetrate bilayer membranes in vitro (36,37).

We speculate that R9C Dyn A may exert its relatively mild neurotoxicity via alternative routes such as inducing membrane leakage via membrane penetration leading to cellular dysfunction (14,36,38) contributing to the inconsistent responses under a specific pre-treatment. R9C Dyn A's relatively mild toxic effects may also be explained by its high oligomerisation properties. Why this does not result in reduced neurotoxicity for R6W Dyn A remains to be investigated; however, we speculate that the non-aggregated R6W Dyn A peptides are more toxic than R9C Dyn A because of alternative mechanisms. Furthermore, the observation that R6W Dyn A toxicity was higher during opioid blockade than following MK801 treatment, supports the hypothesis of opioid-signalling-induced neuroprotection (4).

These data indicate that the partial loss of neuroprotection through opioid signalling may contribute to the pathogenesis of SCA23. Additionally, as in SCA23 elevated levels of R6W Dyn A were observed, it is likely that the increase in peptide contributes to increased toxicity (16).

In conclusion, the R6W and R9C Dyn A peptides reflect gain-of-function mutations, leading to increased peptide stability and decreased peptide solubility, whereas the L5S mutation seemingly induced a loss of function, indicated by the enhanced peptide degradation. This work further supports our previous data, in which L5S Dyn A did not display increased toxicity in primary neuronal cultures, while R6W and R9C Dyn A showed high toxicity. Additionally, the patient carrying the L5S mutation exhibited an age of onset of 73 years, and only a mild ataxic phenotype (2), further strengthening our finding. Overall,

Table 1. Summary of the effects of SCA23 mutations on peptide characteristics

versus wt Dyn A	α-Helix	Membrane positioning	Flexibility	KOR affinity	Degradation	Solubility	Toxicity (100 nM)
L5S Dyn A	No	≈	≈	⇓⇓	↑	≈	↓
R6W Dyn A	No	↑	↑	⇓⇓	⇓⇓	⇓⇓	≈
R9C Dyn A	No	≈	↑↑	⇓⇓	⇓⇓	⇓⇓	↓

decreased affinity to KOR, loss of opioid receptor-mediated neuroprotection and potentiation of the NMDA pathway most likely contribute to the pathological actions of SCA23-mutant Dyn A peptides. However, alternative modes of action such as formation of pores in membranes or interactions with AMPA-receptors or ASICs were not excluded and need further investigation. Interfering with both opioid and NMDA signalling routes should be considered as potential therapeutic strategies for SCA23.

Supplementary Material

Supplementary Material is available at *HMG* online.

Acknowledgements

Funding

References

1. Verbeek, D.S., van de Warrenburg, B.P., Wesseling, P., Pearson, P.L., Kremer, H.P. and Sinke, R.J. (2004) Mapping of the SCA23 locus involved in autosomal dominant cerebellar ataxia to chromosome region 20p13-12.3. *Brain*, **127**, 2551–2557.
2. Bakalkin, G., Watanabe, H., Jezierska, J., Depoorter, C., Verschuuren-Bemelmans, C., Bazov, I., Artemenko, K.A., Yakovleva, T., Dooijes, D., Van de Warrenburg, B.P.C. *et al.* (2010) Prodynorphin mutations cause the neurodegenerative disorder spinocerebellar ataxia type 23. *Am. J. Hum. Genet.*, **87**, 593–603.
3. Schwarzer, C. (2009) 30 Years of Dynorphins–new insights on their functions in neuropsychiatric diseases. *Pharmacol. Ther.*, **123**, 353–370.
4. Hauser, K.F., Aldrich, J.V., Anderson, K.J., Bakalkin, G., Christie, M.J., Hall, E.D., Knapp, P.E., Scheff, S.W., Singh, I.N., Vissel, B. *et al.* (2005) Pathobiology of dynorphins in trauma and disease. *Front. Biosci.*, **10**, 216–235.
5. Chavkin, C. (2013) Dynorphin–still an extraordinarily potent opioid peptide. *Mol. Pharmacol.*, **83**, 729–736.
6. Altier, C. and Zamponi, G.W. (2006) Opioid, cheating on its receptors, exacerbates pain. *Nat. Neurosci.*, **9**, 1465–1467.
7. Tan-No, K., Cebers, G., Yakovleva, T., Hoon Goh, B., Gileva, I., Reznikov, K., Aguilar-Santelises, M., Hauser, K.F., Terenius, L. and Bakalkin, G. (2001) Cytotoxic effects of dynorphins through nonopioid intracellular mechanisms. *Exp. Cell Res.*, **269**, 54–63.
8. Hauser, K.F., Knapp, P.E. and Turbek, C.S. (2001) Structure–activity analysis of dynorphin A toxicity in spinal cord neurons: intrinsic neurotoxicity of dynorphin A and its carboxyl-terminal, nonopioid metabolites. *Exp. Neurol.*, **168**, 78–87.
9. Woods, A.S., Kaminski, R., Oz, M., Wang, Y., Hauser, K., Goody, R., Wang, H.Y.J., Jackson, S.N., Zeitz, P., Zeitz, K.P., *et al.* (2006) Decoy peptides that bind dynorphin noncovalently prevent NMDA receptor-mediated neurotoxicity. *J. Proteome Res.*, **5**, 1017–1023.
10. Przewlocki, R., Parsons, K.L., Sweeney, D.D., Trotter, C., Netzeband, J.G., Siggins, G.R. and Gruol, D.L. (1999) Opioid enhancement of calcium oscillations and burst events involving NMDA receptors and l-type calcium channels in cultured hippocampal neurons. *J. Neurosci.*, **19**, 9705–9715.
11. Wagner, J.J., Caudle, R.M. and Chavkin, C. (1992) Kappa-opioids decrease excitatory transmission in the dentate gyrus of the guinea pig hippocampus. *J. Neurosci.*, **12**, 132–141.
12. Lapalu, S., Moisand, C., Mazarguil, H., Cambois, G., Mollereau, C. and Meunier, J.C. (1997) Comparison of the structure–activity relationships of nociceptin and dynorphin A using chimeric peptides. *FEBS Lett.*, **417**, 333–336.
13. Schlechtingen, G., DeHaven, R.N., Daubert, J.D., Cassel, J.A., Chung, N.N., Schiller, P.W., Taulane, J.P. and Goodman, M. (2003) Structure–activity relationships of dynorphin a analogues modified in the address sequence. *J. Med. Chem.*, **46**, 2104–2109.
14. Sankararamakrishnan, R. and Weinstein, H. (2000) Molecular dynamics simulations predict a tilted orientation for the helical region of dynorphin A(1-17) in dimyristoyl-phosphatidylcholine bilayers. *Biophys. J.*, **79**, 2331–2344.,
15. Hassan, S.A., Mehler, E.L., Zhang, D. and Weinstein, H. (2003) Molecular dynamics simulations of peptides and proteins with a continuum electrostatic model based on screened Coulomb potentials. *Proteins*, **51**, 109–125.
16. Smeets, C.J.L.M., Jezierska, J., Watanabe, H., Duarri, A., Fokkens, M.R., Meijer, M., Zhou, Q., Yakovleva, T., Boddeke, E., den Dunnen, W. *et al.* (2015) Elevated mutant dynorphin A causes Purkinje cell loss and motor dysfunction in spinocerebellar ataxia type 23. *Brain*, **138**, 2537–2552.
17. Pronk, S., Páll, S., Schulz, R., Larsson, P., Bjelkmar, P., Apostolov, R., Shirts, M.R., Smith, J.C., Kasson, P.M., van der Spoel, D. *et al.* (2013) GROMACS 4.5: a high-throughput and highly parallel open source molecular simulation toolkit. *Bioinformatics*, **29**, 845–854.
18. Berger, O., Edholm, O. and Jähnig, F. (1997) Molecular dynamics simulations of a fluid bilayer of dipalmitoylphosphatidyl-choline at full hydration, constant pressure, and constant temperature. *Biophys. J.*, **72**, 2002–2013.
19. Berendsen, H.J.C., Postma, J.P.M., van Gunsteren, W.F., DiNola, A. and Haak, J.R. (1984) Molecular dynamics with coupling to an external bath. *J. Chem. Phys.*, **81**, 3684.
20. Marrink, S.J., Risselada, H.J., Yefimov, S., Tieleman, D.P. and de Vries, A.H. (2007) The MARTINI force field: coarse grained

model for biomolecular simulations. *J. Phys. Chem. B*, **111**, 7812–7824.

21. Tessmer, M.R. and Kallick, D.A. (1997) NMR and structural model of dynorphin A (1-17) bound to dodecylphosphocholine micelles. *Biochemistry*, **36**, 1971–1981.

22. Rzepiela, A.J., Schäfer, L.V., Goga, N., Risselada, H.J., De Vries, A.H. and Marrink, S.J. (2010) Reconstruction of atomistic details from coarse-grained structures. *J. Comput. Chem.*, **31**, 1333–1343.

23. Joosten, R.P., te Beek, T.A.H., Krieger, E., Hekkelman, M.L., Hooft, R.W.W., Schneider, R., Sander, C. and Vriend, G. (2011) A series of PDB related databases for everyday needs. *Nucleic Acids Res.*, **39**, D411–D419.

24. Humphrey, W., Dalke, A. and Schulten, K. (1996) VMD: visual molecular dynamics. *J. Mol. Graph.*, **14**, 33–38. 27–8.

25. Dooley, C.T., Ny, P., Bidlack, J.M. and Houghten, R.A. (1998) Selective ligands for the mu, delta, and kappa opioid receptors identified from a single mixture based tetrapeptide positional scanning combinatorial library. *J. Biol. Chem.*, **273**, 18848–18856.

26. Stargardt, A. and Reits, E. (2013) Kinetic studies of cytoplasmic antigen processing and production of MHC class I ligands. *Methods Mol. Biol.*, **960**, 41–51.

27. Krämer, D. and Minichiello, L. (2010) Cell culture of primary cerebellar granule cells. *Methods Mol. Biol.*, **633**, 233–239.

28. Akkuratov, E.E., Lopacheva, O.M., Kruusmägi, M., Lopachev, A.V., Shah, Z.A., Boldyrev, A.A. and Liu, L. (2015) Functional interaction between Na/K-ATPase and NMDA receptor in cerebellar neurons. *Mol. Neurobiol.*, **52**, 1726–1734.

29. O'Connor, C., White, K.L., Doncescu, N., Didenko, T., Roth, B.L., Czaplicki, G., Stevens, R.C., Wüthrich, K. and Milon, A. (2015) NMR structure and dynamics of the agonist dynorphin peptide bound to the human kappa opioid receptor. *Proc. Natl. Acad. Sci. U. S. A.*, **112**, 11852–11857.

30. Uezono, T., Toraya, S., Obata, M., Nishimura, K., Tuzi, S., Saitô, H. and Naito, A. (2005) Structure and orientation of dynorphin bound to lipid bilayers by 13C solid-state NMR. *J. Mol. Struct.*, **749**, 13–19.

31. Walker, J.M., Moises, H.C., Coy, D.H., Baldrighi, G. and Akil, H. (1982) Nonopiate effects of dynorphin and des-Tyr-dynorphin. *Science*, **218**, 1136–1138.

32. Reits, E., Neijssen, J., Herberts, C., Benckhuijsen, W., Janssen, L., Drijfhout, J.W. and Neefjes, J. (2004) A major role for TPPII in trimming proteasomal degradation products for MHC class I antigen presentation. *Immunity*, **20**, 495–506.

33. Kaspari, A., Diefenthal, T., Grosche, G., Schierhorn, A. and Demuth, H.U. (1996) Substrates containing phosphorylated residues adjacent to proline decrease the cleavage by proline-specific peptidases. *Biochim. Biophys. Acta*, **1293**, 147–153.

34. Singh, I., Goody, R., Goebel, S., Martin, K., Knapp, P., Marinova, Z., Hirschberg, D., Yakovleva, T., Bergman, T., Bakalkin, G. *et al.* (2003) Dynorphin A (1–17) induces apoptosis in striatal neurons *in vitro* through α-amino-3-hydroxy-5-methylisoxazole-4-propionate/kainate receptor-mediated cytochrome C release and caspase-3 activation. *Neuroscience*, **122**, 1013–1023.

35. Sherwood, T.W. and Askwith, C.C. (2009) Dynorphin opioid peptides enhance acid-sensing ion channel 1a activity and acidosis-induced neuronal death. *J. Neurosci.*, **29**, 14371–14380.

36. Madani, F., Taqi, M.M., Wärmländer, S.K.T.S., Verbeek, D.S., Bakalkin, G. and Gräslund, A. (2011) Perturbations of model membranes induced by pathogenic dynorphin A mutants causing neurodegeneration in human brain. *Biochem. Biophys. Res. Commun.*, **411**, 111–114.

37. Bjorneras, J., Graslund, a and Maler, L. (2013) Membrane interaction of disease-related Dynorphin A variants. *Biochemistry*, **52**, 4157–4167.

38. Maximyuk, O., Khmyz, V., Lindskog, C.J., Vukojević, V., Ivanova, T., Bazov, I., Hauser, K.F., Bakalkin, G. and Krishtal, O. (2015) Plasma membrane poration by opioid neuropeptides: a possible mechanism of pathological signal transduction. *Cell Death Dis.*, **6**, e1683.